Numerical Computational of Blood Flow and Mass Transport in Stenosed Bifurcated Artery

Kannigah Thirunanasambantham[1], Zuhaila Ismail[1,*], Lim Yeou Jiann[2], Amnani Shamjuddin[2]

[1] Department of Mathematical Sciences, Faculty of Science, Universiti Teknologi Malaysia, 81310, Johor Bahru, Malaysia
[2] Chemical Reaction Engineering Group (CREG), Faculty of Chemical Engineering and Energy Engineering, University Teknologi Malaysia, 81310, Johor Bahru, Malaysia

ARTICLE INFO

ABSTRACT

Stenosis refers to the narrowing of blood vessels caused by atherosclerosis, which can lead to serious circulatory problems by obstructing blood flow and mass transfer to other organs and tissues in the body. The objective of this investigation is to numerically examine the mass transfer of blood flow in a stenosed bifurcated artery using COMSOL Multiphysics, based on the finite element method. The study takes into account the geometry of a bifurcated artery with stenosis present at the mother and daughter arteries. The blood vessel is modeled as a two-dimensional (2D) rigid wall, and the blood flow is assumed to follow a non-Newtonian Carreau fluid model, being incompressible, laminar, and steady. The continuity equation, momentum equation, and mass transfer equation, along with boundary conditions, will be solved using COMSOL Multiphysics based on the finite element method. The simulation results show that the formation of recirculation zones, as indicated by streamline patterns and mass concentration, can significantly impact the severity of stenosis and Reynolds numbers. Thus, individuals exposed to such recirculation zones may be at risk of developing cardiovascular diseases.

1. Introduction

Coronary artery disease (CAD) is a serious and often deadly medical condition that affects the heart. Study shows that CAD is one of the leading causes of death in industrialized countries [1]. This is because CAD occurs when the coronary arteries, which are the blood vessels that supply oxygen and nutrients to the heart muscle, become narrow or blocked. The cause of this narrowing or blockage is due to the build-up of fats, cholesterol, and other substances within the walls of the coronary arteries [2,3]. This is known as atherosclerosis. This disease may occur from large to medium size arteries involving complex interactions between the arterial wall and the blood flow. The cholesterol present in the blood is normally in the form of low-density lipoproteins (LDLs) where if it started to build up along the arterial wall it is the prime cause of atherosclerosis which leads to

---

stenosis [4]. Plaques, or build-up of material within the arteries, tend to form in areas where there is a change in the curvature of the blood vessels, such as at bends, branches, and bifurcations [3]. These changes in vessel geometry result in a dynamic and disturbed flow pattern, which contributes to the development of stenoses and the progression of atherosclerosis [5]. Additionally, the geometry of the arteries and the location of stenoses may play a crucial role in determining the impact of hemodynamics on the formation of stenoses [6,7].

The non-Newtonian Carreau fluid model is a combination of Newtonian and power law models [8]. As a matter of fact, the fluid model can describe both shear thinning and shear thickening phenomena. The Carreau model was employed in research studies to investigate and compare Newtonian and non-Newtonian behaviors in the common carotid artery with stenoses [9]. They found a trend in the difference in luminal concentration as a function of time which is due to the diffusion mechanism [10,11]. Moreover, different fluids with varying viscosity properties generate eddies or recirculation flow at post-stenotic regions of different sizes. The shear-thinning fluid produces the largest eddies, followed by the Newtonian fluid, while the shear-thickening fluid generates the smallest eddies [12,13]. As a result, for high shear rate regions and input velocity, the Carreau model has been shown to represent wall shear stress (WSS) better than the other models [14]. Not only that, but the model is also useful in both Newtonian and non-Newtonian where the viscosity depends on the shear rate and excelled from low to high range shear [11-15]. As a result, it is reasonable to consider the Carreau model as best suited to represent blood viscosity in the bifurcated which is a combination of the larger mother artery and the smaller daughters' artery.

The primary objective of this research is to investigate the effect of blood flow and mass transport in the stenosed bifurcated artery numerically using COMSOL Multiphysics 5.2 based on the FEM method. Also, investigating the streamline patterns and mass concentration for different Reynolds numbers and stenosis severity can significantly impact the formation of the recirculation zone.

According to the research studies that have been reviewed and analyzed, this research aims to examine the blood flow and mass transfer characteristics in a bifurcated artery with mild stenoses. Studies have been done solely on blood flow on the bifurcated artery, however, mass transfer as mentioned above plays a crucial role in providing a more accurate analysis. Motivated by all those studies mentioned This research attempts to analyze blood flow and mass transport in the stenosed bifurcated artery. The fluid flow is considered incompressible, two-dimensional, steady, and laminar by using parameters as proposed [2]. The blood is treated as non-Newtonian fluid following the Carreau model. The artery is modeled as a rigid wall with no-slip condition. As a numerical computation, COMSOL Multiphysics based on the finite element method will be used to solve the continuity equation, momentum equation, and mass transfer equation together with the boundary conditions.

2. Problem Formulation

To define the computational domain of the bifurcated artery with the presence of stenoses, the following assumptions are made:
  i.   The artery that forms the bifurcation has a finite length.
  ii.   The artery consists of stenosis located in the parent vessel and ostium of bifurcation.
  iii.   To avoid any discontinuities or separation zones, curvatures are introduced at the lateral junctions and the flow divider of the bifurcation.
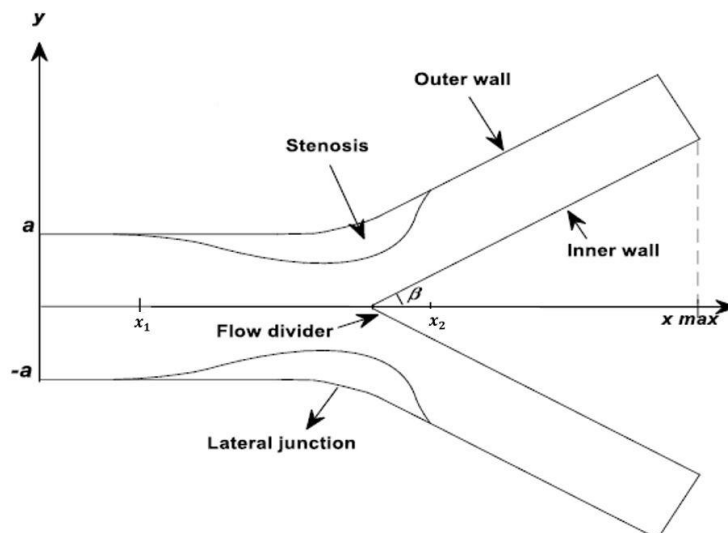
Fig. 1. Geometry of stenosed arterial bifurcation model [3,4,16,17]

2.1 Governing Equations

In this study, the blood in the stenotic bifurcated artery is considered two-dimensional, steady, laminar, and incompressible. The blood is treated as non-Newtonian fluid following the Carreau model to represent the rheological features of flowing blood in a narrow artery. The artery is modeled as a rigid wall with no-slip condition.

The continuity equation is governed as

$$\frac{\partial u}{\partial x} + \frac{\partial v}{\partial y} = 0.$$
(1)

Similarly, the momentum equation in the x and y direction of the Cartesian plane and the shear stress τ take the following form in the Carreau fluid model [11,18],

$$\nabla \cdot (\rho u \vec{V}) = -\frac{\partial p}{\partial x} + \frac{\partial \tau_{xx}}{\partial x} + \frac{\partial \tau_{yx}}{\partial y} + \frac{\partial \tau_{zx}}{\partial z}$$
(2)

$$\nabla \cdot (\rho u V) = -\frac{\partial p}{\partial y} + \frac{\partial \tau_{xy}}{\partial x} + \frac{\partial \tau_{yy}}{\partial y} + \frac{\partial \tau_{zy}}{\partial z},$$
(3)

where,

$$\tau_{xx} = 2\left[\mu_\infty + (\mu_0 - \mu_\infty)\left\{ 1 + \Gamma^2\left[2\left(\left(\frac{\partial u}{\partial x}\right)^2 + \left(\frac{\partial v}{\partial y}\right)^2 \right) \right] \right\}^{\frac{n-1}{2}} \right]\left(\frac{\partial u}{\partial x}\right),$$
(4)

$$\tau_{yx} = \mu_\infty + (\mu_0 - \mu_\infty)\left\{1 + \Gamma^2\left[2\left(\left(\frac{\partial u}{\partial x}\right)^2 + \left(\frac{\partial v}{\partial y}\right)^2\right)\right]\right\}^{\frac{n-1}{2}}\left(\frac{\partial v}{\partial x} + \frac{\partial u}{\partial y}\right), \tag{5}$$

$$\tau_{yy} = 2\left[\mu_\infty + (\mu_0 - \mu_\infty)\left\{1 + \Gamma^2\left[2\left(\left(\frac{\partial u}{\partial x}\right)^2 + \left(\frac{\partial v}{\partial y}\right)^2\right)\right]\right\}^{\frac{n-1}{2}}\right]\left(\frac{\partial v}{\partial y}\right). \tag{6}$$

The mass equation based on Fick's first law is derived as.

$$\left[u\frac{\partial C}{\partial x} + v\frac{\partial C}{\partial y}\right] - D\left(\frac{\partial^2 C}{\partial x^2} + \frac{\partial^2 C}{\partial y^2}\right) = 0. \tag{7}$$

Here u and v are the components of velocity in the x and y directions, $\vec{V}$ is the flow velocity, p is the pressure, and ρ is the density. Based on [18], μ_∞ is the infinite shear rate viscosity, μ_0 is the zero shear rate viscosity, Γ is the time constant, n is the power law index, and τ is the shear stress. D is denoted as mass diffusivity or the diffusion coefficient, as it depends on the mixture's components, temperature, and more. Whereas, C is denoted as the concentration of the component in a mixture.

2.2 Dimensionless Formulation of the Problem

The solution procedure involves the non-dimensionalization method to solve this problem of blood flow and mass transport in the bifurcated artery. The following non-dimensionless quantities are introduced below,

$$u = \frac{u^*}{U_0}, \quad v = \frac{v^*}{U_0}, \quad x = \frac{x^*}{L}, \quad y = \frac{y^*}{L}, \quad P = \frac{P^*}{\rho^* U_0^2} \text{ or } \frac{P^* L}{\mu U_0}, \quad C = \frac{C^*}{C_0}. \tag{8}$$

where U_0 is the reference velocity which represents the average mean inflow velocity, L is the reference length which refers to the length of the inlet, and C_0.refers to the reference concentration [12]. The equation introducing the dimensionless variables with the symbol (*) denotes the dimensionless form to show the differences. However, the symbol (*) can be dropped to represent the dimensionless governing equations.

Eq. (1)-(3) and Eq. (7) after dropping the stars,

$$\frac{\partial u}{\partial x} + \frac{\partial v}{\partial y} = 0, \tag{9}$$

$$u\frac{\partial u}{\partial x} + v\frac{\partial u}{\partial y} = -\frac{\partial P}{\partial x} + \frac{1}{Re}\left[1 + \frac{(\mu_0 - \mu_\infty)}{\mu_\infty}\left\{1 + \Gamma^2\left[2\left(\left(\frac{\partial u}{\partial x}\right)^2 + \left(\frac{\partial u}{\partial y}\right)^2\right)\right]\right\}^{\frac{n-1}{2}}\right]\left[\frac{\partial^2 u}{\partial x^2} + \frac{\partial^2 u}{\partial y^2}\right], \tag{10}$$

$$u\frac{\partial v}{\partial x}+v\frac{\partial v}{\partial y}=-\frac{\partial P}{\partial y}+\frac{1}{\text{Re}}\left[1+\frac{(\mu_0-\mu_\infty)}{\mu_\infty}\left\{1+\Gamma^2\left[2\left(\left(\frac{\partial u}{\partial x}\right)^2+\left(\frac{\partial v}{\partial y}\right)^2\right)\right]\right\}^{\frac{n-1}{2}}\right]\left[\frac{\partial^2 v}{\partial x^2}+\frac{\partial^2 v}{\partial y^2}\right],\tag{11}$$

$$\left[\frac{\partial C}{\partial x}+v\frac{\partial C}{\partial y}\right]=\frac{1}{\text{ReSc}}\left(\frac{\partial^2 C}{\partial x^2}+\frac{\partial^2 C}{\partial y^2}\right).\tag{12}$$

By employing the non-dimensionalization procedure, the non-dimensional parameters such as Reynolds number, Re, and Schmidt number Sc are obtained as,

$$\text{Re}=\frac{\rho U_0 L}{\mu}\text{ and }\text{Sc}=\frac{\mu}{\rho D}\tag{13}$$

2.3 Boundary Conditions

At the inlet, a parabolic velocity profile is imposed, where a fully developed velocity profile is taken place as follows[5,19]:

$$u(x,y)=u_{\max}\left(1-\left(\frac{y^2}{a^2}\right)^{\frac{n+1}{n}}\right)\text{ and }v(x,y)=0,\text{ at }x=0\text{ and }-a\le y\le a,n=1\tag{14}$$

Next, no-slip conditions along the walls of the artery:

$$u(x,y)=0,\ v(x,y)=0.\tag{15}$$

Then, at the outlet, a traction-free condition is applied with no tangential and normal forces as follows:

$$\left(-pI+\tau\right).\boldsymbol{n}=0,\tag{16}$$

where τ is the stress tensor, $\boldsymbol{n}$ is a unit outward normal vector with the pressure point constraint $p=0$ applied at $x=0$ and $y=0.0075$.

The condition for mass concentration along the axis of symmetry is proposed as follows,

$$\frac{\partial C(x,y)}{\partial y}=0\text{ on }y=0.\tag{17}$$

The inlet mass concentration of the solute is assumed to be constant, whereas the outlet boundary of the artery of finite length $x_{\max}$ is considered to have zero concentration gradient, which can be expressed non-dimensionally as,

$$C(x,y)=1 \ at \ x=0 \ and \ \frac{\partial C(x,y)}{\partial x}=0 \ at \ x=x_{\max}. \qquad (18)$$

A Dirichlet boundary condition of zero concentration on the arterial wall is defined as

$$C(x,y)=0, \qquad (19)$$

This shows, Eq. (19) effectively ignores the connection between mass transport in the blood and mass transport in the arterial wall, i.e., zero concentration on the wall is suitable when the fluid-side mass transport resistance dominates the wall-side opposition, as shown by [20]. Except at the inlet, where the solute's initial mass concentration has been considered zero.

$$C(x,y)=0 \ \ for \ x>0. \qquad (20)$$

3. Computational Mesh and Model Validation

The governing equations subjected to the boundary conditions mentioned above are solved using the commercial software package COMSOL Multiphysics 5.2. All computations are performed on a computer running 64-bit Windows 10 with a speed of 2667MHz and 7.89GB of RAM. Several mesh refinement attempts were conducted to ensure the results were not dependent on the mesh parameters. The number of domain elements and the maximum velocity were computed using COMSOL Multiphysics, as shown in Table 1.

Table 1
Mesh Parameters and Total Domain Elements

Software	Parameter	Domain Element	Maximum Velocity (m/s)
Present Study, COMSOL	Mesh 1	2385	0.13074
	Mesh 2	4118	0.13280
	Mesh 3	7212	0.13429
	Mesh 4	16933	0.13542

Mesh 4 with domain element 16933 is selected to obtain more accurate and satisfactory results. The mesh results obtained are consistent with [19]. Using the same parameters [19,21], Figure 2 matches with previous researchers; thus, accurate and satisfactory results can be achieved to solve the problem.

Based on the mesh dependency test illustrated in Table 1, Figure 2, and Figure 3, the maximum velocity for all mesh is almost similar, with small differences of approximately 0.00011 m/s. Based on the graph in Figure 2, Mesh 1 and Mesh 2 are distorted and do not have a smooth curve. However, Mesh 3 and Mesh 4 produce smoother and constant curves. Therefore, Mesh 4 with domain element 16933 is selected to obtain more accurate and satisfactory results.
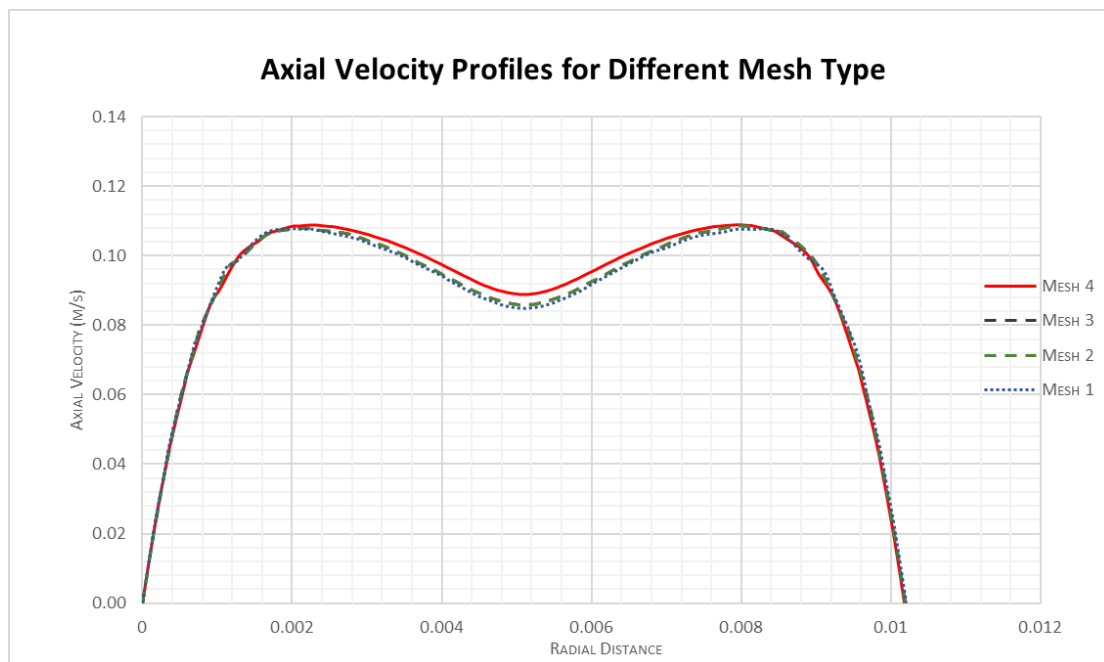
Fig. 2. Axial velocity profiles with different numbers of domain elements at x=0.02 m

(a) Mesh 1

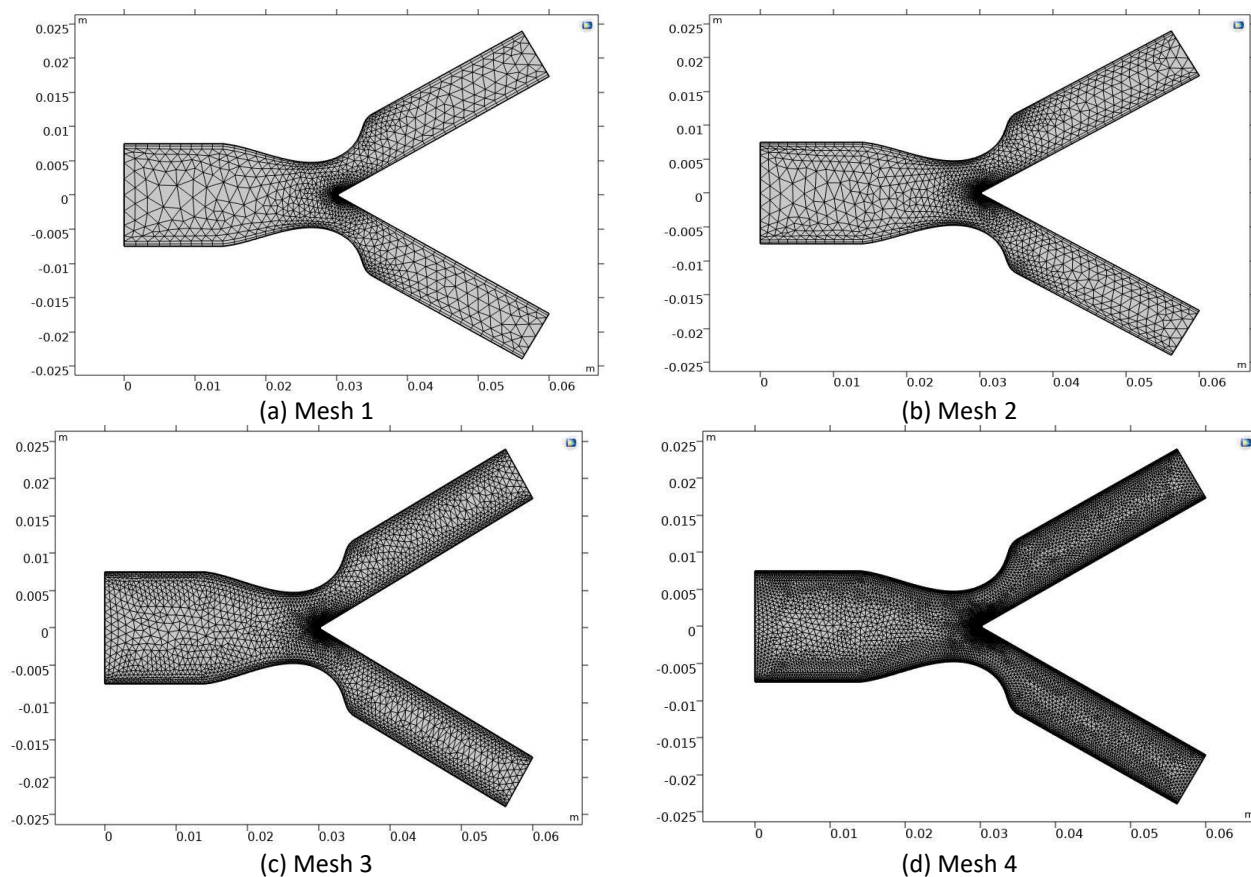(b) Mesh 2

(c) Mesh 3

(d) Mesh 4

Fig. 3. Different unstructured triangular mesh

The geometry is constructed based on the model proposed by [11,22,23] for validation purposes. Let (x, y) be the coordinates of a material point, then

$$R_1(x) = \begin{cases} a, & 0 \le x \le d \text{ and } d + l_0 \le x \le x_1, \\ a - \dfrac{4\tau_m}{l_0}\left\{l_0(x-d)-(x-d)^2\right\}, & d \le x \le d + l_0, \\ a + r_0 - \sqrt{r_0^2 - (x-x_1)^2}, & x_1 \le x \le x_2, \\ 2r_1 \sec\beta + (x-x_2)\tan\beta, & x_2 \le x \le x_{max} - s \end{cases} \tag{21}$$

$$R_2(x) = \begin{cases} 0, & 0 \le x \le x_3, \\ \sqrt{r'_0 - (x-(x_3+r'_0))^2}, & x_3 \le x \le x_4, \\ r'_0 \cos\beta + (x-x_4)\tan\beta, & x_4 \le x \le x_{max}, \end{cases} \tag{22}$$

where the outer wall $R_1(x)$ and inner wall geometry $R_2(x)$, respectively. The radii of curvature for the lateral and offset of the lateral junction are denoted by r_0 and r'_0 respectively. The length of stenosis at a distance from the origin is indicated by l_0. The location of the onset and offset of the lateral junction is denoted by x_1 and x_2 respectively. The apex is indicated as x_3 and τ_m represents the maximum height of stenosis occurring at $d + \dfrac{l_0}{6}$ and $d + \dfrac{5l_0}{6}$ while β denoted as half of the bifurcation angle. The given values can specify the parameters involved in the above Eq. (21) and Eq. (22).

$$x_2 = x_1 + r_0 \sin\beta, \quad r_0 = \frac{a - 2r_1 \sec\beta}{\cos\beta - 1}, \quad r'_0 = \frac{(x_3 - x_2)\sin\beta}{1 - \sin\beta}, \tag{23}$$

$$x_3 = x_2 + q, \quad s = 2r_1 \sin\beta, \tag{24}$$

where q is considered a small number between the range $0.0001 \le q \le 0.0005$ chosen for the compatibility of the geometry and

$$x_4 = x_3 + r_0(1 - \sin\beta). \tag{25}$$

The dimensional data for validation purposes is used following [11,22],

$a = 0.0075m, \ l_0 = 0.015m, \ d = 0.005m, \ x_{max} = 0.06m$

$x_1 = 0.025m, \ \rho = 1050 kgm^{-3}, \ \mu = 0.0035 Pas^{-1}, \ \beta = 30°$

$q = 0.0002m, \ r_1 = 0.51a, \ \tau_m = 0.4a, 0.6a, 0.8a.$

Figure 4 shows the result of the velocity profile obtained from COMSOL Multiphysics 5.2 at x =0.0125m, which is at the maximum constriction. Figure 4 is compared with [19] for validation purposes, and the results are produced similarly. To achieve the outcome in COMSOL. Reynold's number was set to 285.
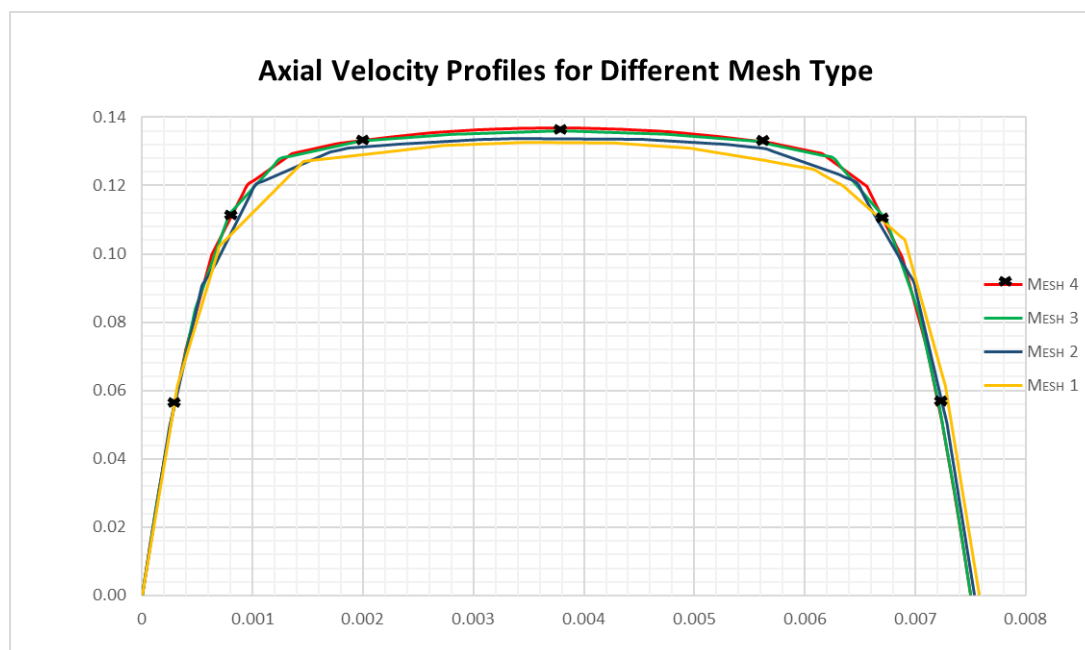
Fig. 4. Axial velocity profiles with different numbers of domain elements at x=0.0125 m

Mesh 4 with domain element 17269 is selected to obtain more accurate and satisfactory results. The mesh results obtained are consistent with [19]. Using the same parameters [19,24], Figure 4 matches with previous researchers; thus, accurate and satisfactory results can be achieved for this problem.

4. Results and Discussion

By applying COMSOL Multiphysics based on the FEM method, velocity profiles at the mother and daughter artery and mass concentration are analyzed by differing Reynolds numbers and the severity of the stenosis. To have a thorough quantitative analysis of the effects of non-Newtonian Carreau blood rheology on the stenotic bifurcated artery flow streamlines, axial velocity, and mass concentration are performed.

4.1 Axial Velocity Profile for Different Reynolds Numbers

Figure 5 shows the velocity profile of the bifurcated artery with Reynolds numbers of Re=300 and Re=500 at the position of x=0.03m nearby to the central passage of the bifurcated artery. Based on Figure 5, the velocity profile increases significantly as the artery narrows. In Figure 5, as the Reynold number increases, the velocity of the artery increases. The velocity profile of the lower Reynolds number Re=300 is lower and flatter than the velocity profile at Re=500. This is due to the increased inertial force due to the higher flow rate when the Reynold number increases [25]. With a lower Reynolds number, the blood moves slowly along the axial direction near the central axis of the vessel. Comparatively, the findings of the velocity profile are consistent with [11].
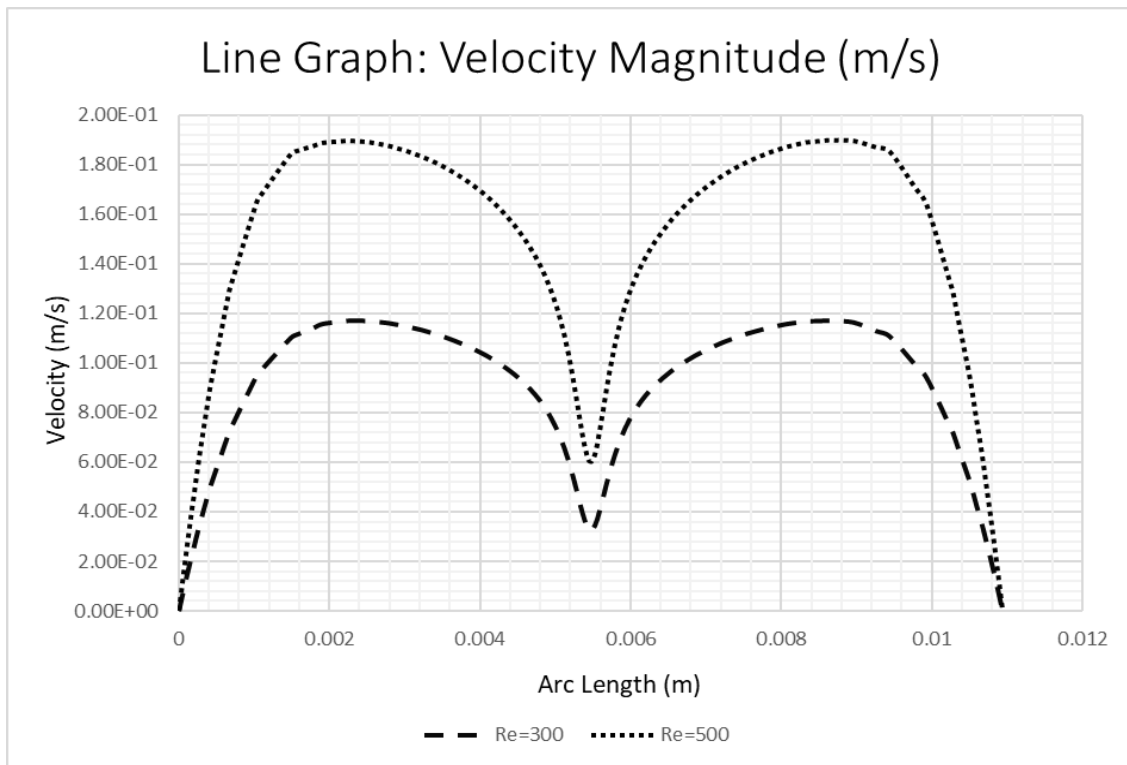
Fig. 5. Axial blood flow velocity with Reynolds number, Re=300 and Re=500 at x=0.03 m

4.2 Mass Concentration for Different Reynolds Numbers

Figure 6 illustrates the concentration C, transfer in the artery with Reynolds number of Re=300 and Re=500. The mass concentration at each axial position converges to zero according to the wall conditions. It can be observed that the flow of mass concentration increases from the wall and remains constant at one throughout the artery and decreases to zero towards the wall. The flow velocity increases as the flow get accelerated toward the throat of stenosis leading to an increase in solute concentration. It can be seen from Figure 6 that the mass concentration at Re=500 increases drastically and decreases slowly compared to the mass concentration at Re=300. It also noted that the accumulation of mass concentration from the wall to the center of stenosis is much higher with a higher Reynolds number value. To summarize, the narrowness of the artery and the impact of Reynolds numbers affect the velocity, leading to an increase or decrease in mass concentration.
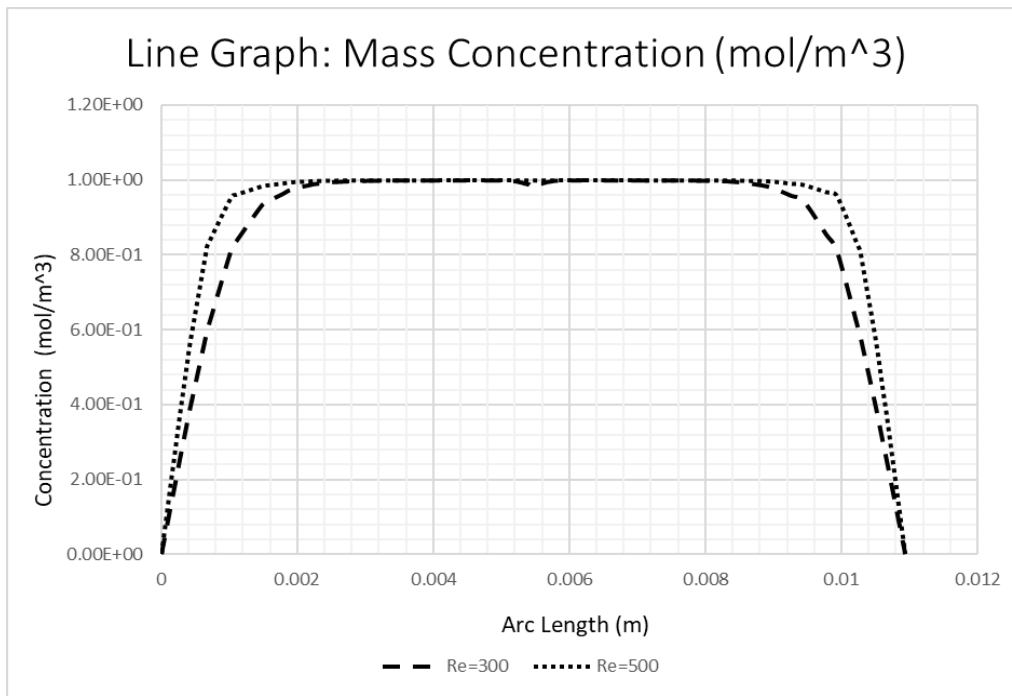
Fig. 6. Mass concentration with Reynolds number, Re=300 and Re=500 at x=0.03 m

4.3 Streamline Pattern for Different Severity of Stenosis

The impact of stenosis on blood flow is further shown in Figure 7(a), (b), (c), and Figure 8, which illustrate the streamline pattern and axial velocity for occlusions of 20%, 40%, and 60% at the parent artery that extends into the upper wall of the bifurcation. The degree of stenosis was calculated using the formula presented below based on [19],

$$\text{Percentage of the severity of stenosis} = \left[1 - \left(\frac{D_{stenosis}}{D_{normal}}\right)\right] \times 100,$$

where $D_{stenosis}$ and D_{normal} represents the diameter of the artery at the most severe site and the diameter of the normal healthy artery, respectively.

The simulation results of velocity magnitude, streamline, and velocity surface of the blood flow of 20%, 40%, and 60% are shown in Figure 7. Figure 7(a) shows streamline behavior with 20% severity which is still normal undisrupted flow. On the other hand, in Figure 7(b), the stenosis with 40% severity, the maximum velocity increases, continuing with the appearance of a recirculation zone at the offset of the stenosis. This also can be seen in Figure 7(c), the maximum velocity of 60% stenosis severity is at the narrow artery with a larger recirculation zone at the post-stenotic region. It is clear from the results shown in Figure 7(c), the reversal flow caused by the vortex crosses the edge of stenosis, as it is unable to follow the curved shape of stenosis and change direction at the same time. This increases the potential for the development of atherosclerosis.
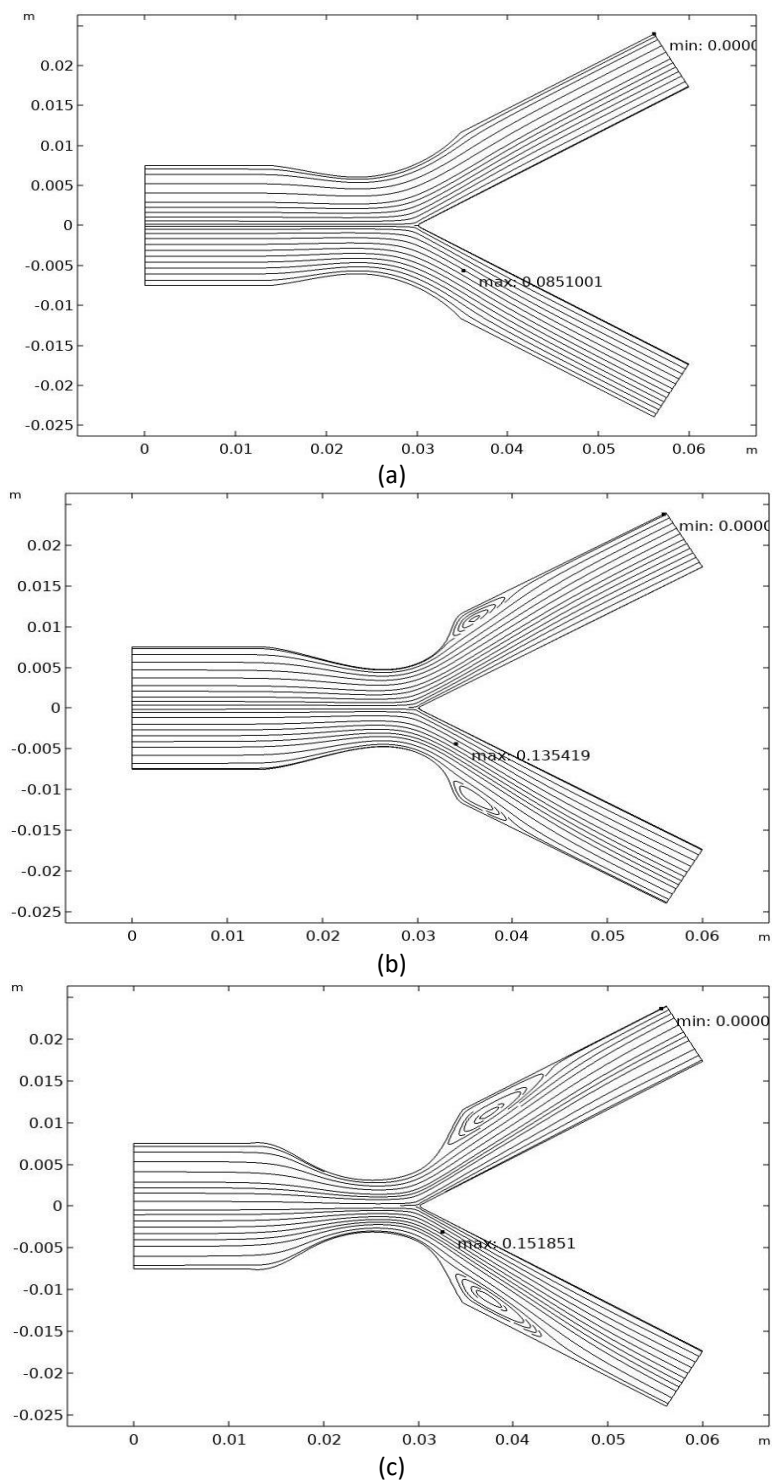
Fig. 7. Streamline pattern of different severity of stenosis (a) 20%, (b) 40%, and (c) 60%

It has been noted in all scenarios that the axial velocity in the stenosis region increases as the area reduction increases. It is notable from Figure 8 that axial velocity differs significantly with increasing severity in the daughter artery, where the stenosis is extended. This also aligns with the results [9,13] where the steep velocity profile was noted at the bifurcation regions and reversal flow at the outer region of the carotid artery. Hence, with a sudden increase in area reduction, a drastic change in values and velocity peaks at the stenosis can be seen. With 40% and 60% severity of stenosis, the trendline of velocity differs slightly as towards the wall surface, the fluid velocity

decreases gradually, rises back, and then decreases to zero. This is due to the occurrence of backflow and an increase in separation flow [18]. In addition, this phenomenon is due to the development of platelet deposition triggered by the formation of separation flow, then leads to the complication of intimal thickening formation [19]. This results in a twisting effect on the blood flow, with the strength of the twisting effect becoming more pronounced further downstream shown in Figure 8. In summary, increased velocity has the potential to elevate wall shear stress, which can lead to potential damage to the endothelial cells lining the blood vessel wall. Consequently, this can contribute to an increased risk of stenosis development [13].
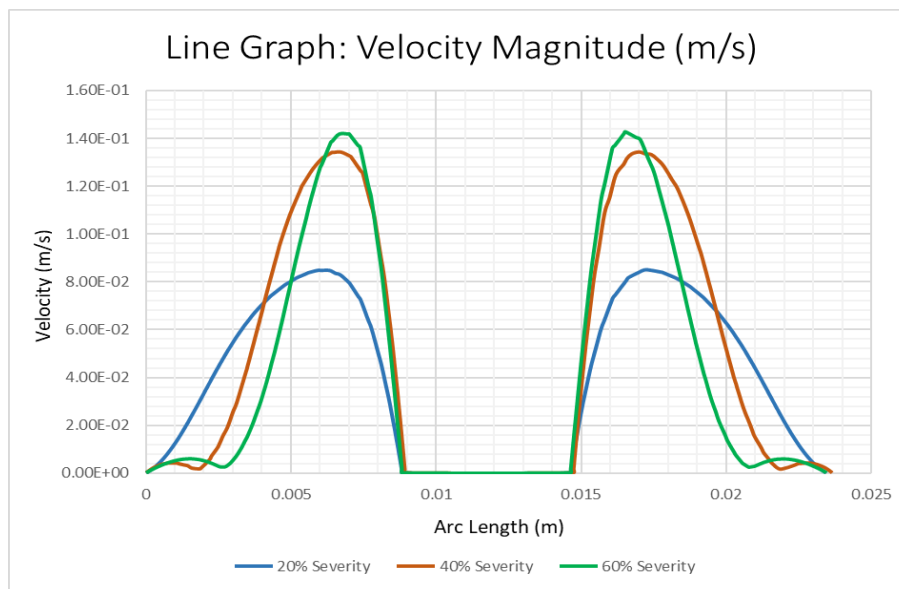

Fig. 8. Axial velocity profiles with different stenosis severity at x=0.035 m

4.4 Mass Concentration for Different Severity of Stenosis

Figure 9 illustrates the concentration C, transfer in the daughter artery with different severity of stenosis consisting of 20%, 40%, and 60% of occlusion area at x=0.035m. Based on Figure 9, as the occlusion area increases, the mass concentration increases and decreases faster due to the narrowness of the artery, which can be seen at 60% and 40% stenosis severity. The flow velocity increases as the flow accelerates toward the daughter artery leading to an increase in solute concentration. At the recirculation zone, a low mass transfer occurs as the region possesses a low-velocity flow and weak recirculation zone, leading to an increase in mass concentration throughout the artery and reducing towards the wall.

It can be seen from Figure 9 that with higher severity, such as 40% and 60% stenosis, the trendline from the artery wall, the mass concentration increases slowly, and it is distorted. Then, towards the artery's center, the mass concentration increases drastically to the value of one. It is noted that the behavior of the concentration at the post-stenotic region gets distorted, which could be due to the separation of flow. The formation of flow reversal and recirculation zones can increase the risk of cardiovascular diseases. The post-stenotic zones are areas where the blood flow slows down, which is particularly concerning for individuals who have atherosclerosis. The stagnant blood in these zones can increase the likelihood of developing complications related to this condition [16,25]. To summarize, the narrowness of the artery or the severity of stenosis affects the velocity, leading to an increase or decrease in mass concentration.
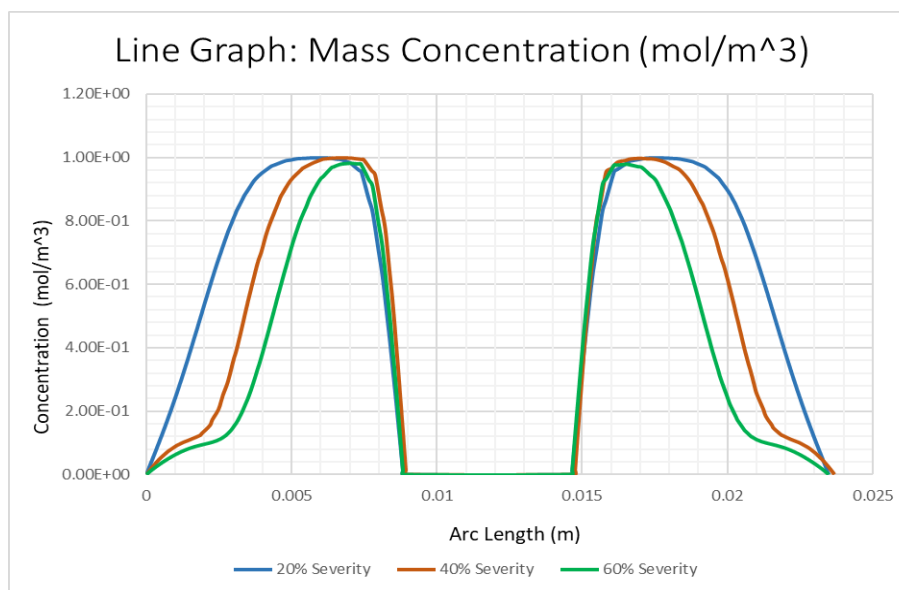
Fig. 9. Mass concentration of different severity of stenosis at x=0.035 m

5. Conclusions

This study focused on blood flow analysis in a stenosed bifurcated artery using the Carreau fluid model. This is important because the flow patterns of blood and the mechanical properties of blood vessels are related to the development of atherosclerosis. Using the Carreau fluid model, the study evaluated the changes in velocity distribution and mass concentration with different Reynolds numbers and different severity of stenosis in the bifurcated artery. The main findings of the present study can be concluded as follows:

i.   The stenosis region showed an increase in axial velocity and a peak in the magnitude of fluid properties.
ii. The magnitude of fluid properties increased as the area reduction increased.
iii. The Reynolds number increases, and the velocity magnitude increases. Thus, with a slight decrease in viscous force with high Re, an increase in velocity streamline with the viscoelastic nature of blood could occur, leading to difficulty in the flow of mass concentration.
iv. As the stenosis is more severe, the mass concentration increases. This is due to the narrowness and the severity of stenosis, leading to an increase in velocity and, subsequently, mass concentration.

These studies provide valuable information for medical practitioners seeking to understand blood flow under stenosis in bifurcated arteries. Thus, with knowledge or understanding of the behavior of mass transfer in arterial blood flow, the treatment of stenotic arteries can be improved, or the likelihood of stenosis occurring after surgery can be reduced. However, it is acknowledged that future studies should consider more anatomically realistic models to understand further the impact of three-dimensional flow patterns on mass transport. The second suggestion is that since blood pressure is favorably influenced by hematocrit, further research should be done to determine how other factors, such as nutrition, smoking, excess weight, and other cardiovascular factors, affect stenosed arteries.

Acknowledgement

References

[1] Malota, Zbigniew, Jan Glowacki, Wojciech Sadowski, and Marcin Kostur. "Numerical analysis of the impact of flow rate, heart rate, vessel geometry, and degree of stenosis on coronary hemodynamic indices." *BMC cardiovascular disorders* 18, no. 1 (2018): 1-16. https://doi.org/10.1186/s12872-018-0865-6

[2] Alsemiry, Reima D., Prashanta K. Mandal, Hamed M. Sayed, and Norsarahaida Amin. "Numerical solution of blood flow and mass transport in an elastic tube with multiple stenoses." *BioMed research international* 2020 (2020). https://doi.org/10.1155/2020/7609562

[3] Jamali, Muhammad Sabaruddin Ahmad, and Zuhaila Ismail. "Simulation of Heat Transfer on blood flow through a stenosed bifurcated artery." *Journal of Advanced Research in Fluid Mechanics and Thermal Sciences* 60, no. 2 (2019): 310-323.

[4] Bhogal, Sukhdeep, Cheng Zhang, Amer I. Aladin, Gary S. Mintz, and Ron Waksman. "Provisional Versus Dual Stenting of Left Main Coronary Artery Bifurcation Lesions (from a Comprehensive Meta-Analysis)." *The American Journal of Cardiology* 185 (2022): 10-17. https://doi.org/10.1016/j.amjcard.2022.09.012

[5] Jamali, Muhammad Sabaruddin Ahmad, Zuhaila Ismail, and Norsarahaida Saidina Amin. "Effect of Different Types of Stenosis on Generalized Power Law Model of Blood Flow in a Bifurcated Artery." *Journal of Advanced Research in Fluid Mechanics and Thermal Sciences* 87, no. 3 (2021): 172-183. https://doi.org/10.37934/arfmts.87.3.172183

[6] Liu, Biyue, and Dalin Tang. "Influence of distal stenosis on blood flow through coronary serial stenoses: a numerical study." *International Journal of Computational Methods* 16, no. 03 (2019): 1842003. https://doi.org/10.1142/S0219876218420033

[7] SARIFUDDIN, Santabrata Chakravarty, and Prashanta Kumar Mandal. "Effect of asymmetry and roughness of stenosis on non-Newtonian flow past an arterial segment." *International Journal of Computational Methods* 6, no. 03 (2009): 361-388. https://doi.org/10.1142/S0219876209001887

[8] Ismail, Zuhaila, Muhammad Sabaruddin Ahmad Jamali, Norliza Mohd Zain, and Lim Yeou Jiann. "Bioheat transfer of Blood Flow on Healthy and Unhealthy Bifurcated Artery: Stenosis." *Journal of Advanced Research in Applied Sciences and Engineering Technology* 28, no. 2 (2022): 56-79. https://doi.org/10.37934/araset.28.2.5679

[9] Ningappa, Abhilash Hebbandi, Suraj Patil, Gowrava Shenoy Belur, Augustine Benjamin Valerian Barboza, Nitesh Kumar, Raghuvir Pai Ballambat, Adi Azriff Basri, Shah Mohammed Abdul Khader, and Masaaki Tamagawa. "Influence of altered pressures on flow dynamics in carotid bifurcation system using numerical methods." *Journal of Advanced Research in Fluid Mechanics and Thermal Sciences* 97, no. 1 (2022): 47-61. https://doi.org/10.37934/arfmts.97.1.4761

[10] Akbar, Noreen Sher, and S. Nadeem. "Carreau fluid model for blood flow through a tapered artery with a stenosis." *Ain Shams Engineering Journal* 5, no. 4 (2014): 1307-1316. https://doi.org/10.1016/j.asej.2014.05.010

[11] Zaman, A., N. Ali, M. Sajid, and T. Hayat. "Effects of unsteadiness and non-Newtonian rheology on blood flow through a tapered time-variant stenotic artery." *AIP advances* 5, no. 3 (2015). https://doi.org/10.1063/1.4916043

[12] Zain, Norliza Mohd, Zuhaila Ismail, and Peter Johnston. "A Stabilized Finite Element Formulation of Non-Newtonian Fluid Model of Blood Flow in A Bifurcated Channel with Overlapping Stenosis." *Journal of Advanced Research in Fluid Mechanics and Thermal Sciences* 88, no. 1 (2021): 126-139. https://doi.org/10.37934/arfmts.88.1.126139

[13] Ramdan, Salman Aslam, Mohammad Rasidi Rasani, Thinesh Subramaniam, Ahmad Sobri Muda, Ahmad Fazli Abdul Aziz, Tuan Mohammad Yusoff Shah Tuan Ya, Hazim Moria, Mohd Faizal Mat Tahir, and Mohd Zaki Nuawi. "Blood Flow Acoustics in Carotid Artery." *Journal of Advanced Research in Fluid Mechanics and Thermal Sciences* 94, no. 1 (2022): 28-44. https://doi.org/10.37934/arfmts.94.1.2844

[14] Khan, Masood, Humara Sardar, M. Mudassar Gulzar, and Ali Saleh Alshomrani. "On multiple solutions of non-Newtonian Carreau fluid flow over an inclined shrinking sheet." *Results in physics* 8 (2018): 926-932. https://doi.org/10.1016/j.rinp.2018.01.021

[15] Subramaniam, Thineshwaran, and Mohammad Rasidi Rasani. "Pulsatile CFD Numerical Simulation to investigate the effect of various degree and position of stenosis on carotid artery hemodynamics." *Journal of Advanced Research in Applied Sciences and Engineering Technology* 26, no. 2 (2022): 29-40. https://doi.org/10.37934/araset.26.2.2940

[16] Ozaltun, B. "Side Branch Occlusion Determinants in Bifurcation Lesions Treated with Provisional Stenting Technique." *Angiol* 6, no. 213 (2018): 2. https://doi.org/10.4172/2329-9495.1000213

[17] Pan, Manuel, Alfonso Medina, José Suárez de Lezo, Miguel Romero, Jose Segura, Pedro Martín, Javier Suárez de Lezo et al. "Coronary bifurcation lesions treated with simple approach (from the Cordoba & Las Palmas [CORPAL]

Kiss Trial)." *The American journal of cardiology* 107, no. 10 (2011): 1460-1465. https://doi.org/10.1016/j.amjcard.2011.01.022

[18]   Kabir, Md Alamgir, Md Ferdous Alam, and M. Ashraf Uddin. "A numerical study on the effects of Reynolds number on blood flow with spiral velocity through regular arterial stenosis." *Chiang Mai J. Sci* 45, no. 6 (2018): 2515-2527.

[19]   Zain, Norliza Mohd, and Zuhaila Ismail. "Modelling of Newtonian blood flow through a bifurcated artery with the presence of an overlapping stenosis." *Malaysian Journal of Fundamental and Applied Sciences* 13, no. 2017 (2017): 304-309. https://doi.org/10.11113/mjfas.v13n4-1.866

[20]   Kaazempur-Mofrad, M. R., S. Wada, J. G. Myers, and C. R. Ethier. "Mass transport and fluid flow in stenotic arteries: axisymmetric and asymmetric models." *International Journal of Heat and Mass Transfer* 48, no. 21-22 (2005): 4510-4517. https://doi.org/10.1016/j.ijheatmasstransfer.2005.05.004

[21]   Abd Aziz, Azyante Erma, Muhammad Sabaruddin Ahmad Jamali, and Zuhaila Ismail. "Numerical simulation of generalized power law blood flow model through different angles of stenosed bifurcated artery." *Journal of Mathematics and Computing Science (JMCS)* 7, no. 2 (2021): 1-14. https://doi.org/10.33292/amm.v1i2.6

[22]   Zain, Norliza Mohd, and Zuhaila Ismail. "Dynamic Response of Heat Transfer in Magnetohydrodynamic Blood Flow Through a Porous Bifurcated Artery with Overlapping Stenosis." *Journal of Advanced Research in Fluid Mechanics and Thermal Sciences* 101, no. 1 (2023): 215-235. https://doi.org/10.37934/arfmts.101.1.215235

[23]   Chakravarty, Santabrata, and Prashanta Kumar Mandal. "An analysis of pulsatile flow in a model aortic bifurcation." *International journal of engineering science* 35, no. 4 (1997): 409-422. https://doi.org/10.1016/S0020-7225(96)00081-X

[24]   Fazli, S., E. Shirani, and M. R. Sadeghi. "Numerical simulation of LDL mass transfer in a common carotid artery under pulsatile flows." *Journal of biomechanics* 44, no. 1 (2011): 68-76. https://doi.org/10.1016/j.jbiomech.2010.08.025

[25]   Owasit, Pinyo, and Somchai Sriyab. "Mathematical modeling of non-Newtonian fluid in arterial blood flow through various stenoses." *Advances in Difference Equations* 2021, no. 1 (2021): 1-20. https://doi.org/10.1186/s13662-021-03492-9